NANOSYSTEMS:
PHYSICS, CHEMISTRY, MATHEMATICS

Original article

Nguyen Pham Quynh Anh *Nanosystems: Phys. Chem. Math.*, 2026, **17** (2), 193–199.
http://nanojournal.ifmo.ru
DOI 10.17586/2220-8054-2026-17-2-193-199

Dispersion analysis and tunable magnetic properties of a biaxial hyperbolic metamaterial based on n-GaAs/AlGaAs heterostructures

Nguyen Pham Quynh Anh

Faculty of Engineering and Technology, Saigon University, Cho Quan Ward, Ho Chi Minh City, Vietnam

npqanh@sgu.edu.vn

ABSTRACT This study presents the design and theoretical analysis of a tunable biaxial hyperbolic metamaterial (BHMM) constructed from a layered n-GaAs/AlGaAs heterostructure under an external magnetic field. The objective is to optimize the tunability in order to control the dispersion shape for applications in the terahertz (THz) frequency regime. The effective medium approximation (EMA) model is employed and demonstrates the coexistence of two wave modes, namely, a closed ellipsoidal and an open hyperboloidal isofrequency surface. The results reveal that the external magnetic field acts as a powerful tuning mechanism, enabling spectral shifting of the dispersion and active switching between Type-I and Type-II hyperbolic regimes. In addition, the conditions required to achieve extreme compression of the isofrequency surface (IFS), which is essential for beam steering control, are analyzed. This compression occurs when one component of the permittivity reaches extremely large values, leading to the formation of near-flat segments on the isofrequency surface.

KEYWORDS biaxial hyperbolic metamaterial, terahertz frequency regime, hyperboloidal isofrequency surface, effective medium approximation

FOR CITATION Nguyen Pham Quynh Anh Dispersion analysis and tunable magnetic properties of a biaxial hyperbolic metamaterial based on n-GaAs/AlGaAs heterostructures. *Nanosystems: Phys. Chem. Math.*, 2026, **17** (2), 193–199.

1. Introduction

The rapid advancement of materials science and nanotechnology has led to the emergence of metamaterials – artificially engineered composite structures exhibiting extraordinary electromagnetic properties that are not found in naturally occurring materials, such as negative refractive index and strongly anisotropic dispersion [1–8]. These materials serve as a fundamental platform for the development of compact, multifunctional photonic and electromagnetic devices, and are particularly significant for applications operating in the terahertz (THz) and infrared (IR) frequency regimes [9, 10].

Among anisotropic materials, hyperbolic metamaterials (HMMs) stand out due to their ability to exhibit strongly anisotropic dispersion. HMMs are characterized by an effective dielectric permittivity tensor ($\hat{\varepsilon}$) with principal components of opposite signs ($\varepsilon_\perp \cdot \varepsilon_\parallel < 0$). This hyperbolic property enables HMMs to support high-wavevector ($k \to \infty$) modes, thereby overcoming the diffraction limit and significantly enhancing the photonic density of states (PDOS) [11,12]. HMMs have attracted considerable attention for a wide range of applications, including hyperlensing, perfect absorption, and terahertz (THz) biosensing [13].

Most current studies have predominantly focused on uniaxial hyperbolic metamaterials (HMMs), for which $\varepsilon_{xx} = \varepsilon_{yy} \neq \varepsilon_{zz}$. Such media exhibit only two singular points (where the two dispersion surfaces intersect, i.e., optical topological transitions or $\varepsilon \to 0/\infty$) along the symmetry axis, leading to iso-frequency surfaces with rotational symmetry around the optical (Z) axis [14]. Although this symmetry simplifies theoretical analysis, it significantly restricts the ability to manipulate wave propagation at arbitrary angles in three-dimensional space. Consequently, the flexibility in controlling energy flow (beam steering) and the multifunctionality of devices remain limited. To extend the controllability of electromagnetic waves in full three-dimensional space, recent research has shifted toward biaxial hyperbolic metamaterials, a class of media characterized by three distinct components of the effective dielectric permittivity tensor ($\varepsilon_{xx} \neq \varepsilon_{yy} \neq \varepsilon_{zz}$). This additional degree of freedom enables more flexible control of the energy flow with respect to the azimuthal angle [15, 16]. These metamaterials can support up to four potential singular points and possess more complex iso-frequency surfaces, thereby enabling multichannel device designs and improved polarization management, which are essential for advanced telecommunication and sensing applications [17].

Semiconductor-dielectric layered structures subjected to an external magnetic field constitute an effective approach for realizing biaxial hyperbolic metamaterials (BHMMs) and enabling magnetic-field tunability of their extreme dispersion characteristics [18]. Owing to their in-plane anisotropy, BHMMs allow significantly enhanced control of electromagnetic energy flow over a wide range of azimuthal angles. Kuznetsov E.V. and co-workers have optimized BHMM designs to achieve highly accurate energy distribution [19]. In recent years, research on biaxial hyperbolic metamaterials has progressed from proof-of-concept demonstrations toward performance optimization and enhanced tunability for practical applications [20].

Research on semiconductor-based hyperbolic metamaterials highlights that while these structures offer unique optical properties like infinite density of states, their performance depends heavily on the carrier concentration and layer thickness. However, a significant discrepancy exists between nominal design parameters and as-grown structures due to physical phenomena such as band bending and depletion effects at the interfaces. To accurately predict optical responses using effective medium theory, these practical changes in material properties must be integrated into the design process for optimized HMM applications [21]. Moreover, the synergistic coupling between the plasma response of heavily doped semiconductors and the phononic resonances of the crystal lattice indicates that hybrid BHMMs can support multiple dispersion regimes, including the biaxial hyperbolic regime, and offer substantially greater tunability than systems relying on a single physical mechanism (e.g., purely plasmonic platforms). This hybrid strategy represents a promising pathway for the development of multifunctional BHMM devices.

Although previous studies have confirmed the effectiveness of biaxial hyperbolic metamaterials (BHMMs) in controlling energy flow and wave propagation direction, a significant research gap remains in the design of BHMM structures that operate efficiently at room temperature while offering high integration capability. To address these challenges and expand the application potential of BHMMs in terahertz (THz) telecommunications and sensing, this work focuses on phase-transition phenomena in a novel n-GaAs/AlGaAs layered structure, an advanced material platform. The objective is to identify optimal operating conditions, including external magnetic field strength and layer thickness ratios that enable precise control over near-flat segments of the iso-frequency surface, thereby optimizing device performance for THz beam steering and sensing applications.

2. Effective model for n-GaAs/AlGaAs-based biaxial hyperbolic metamaterial

We employ the effective medium approximation (EMA) to investigate a novel multilayer system composed of n-GaAs (semiconductor) and AlGaAs (dielectric) layers. This material platform is deliberately chosen to enable room-temperature operation and enhanced integration capability, in contrast to earlier foundational studies that relied primarily on n-InSb and low-temperature operation. The EMA model is applied under the condition that the individual layer thicknesses are much smaller than the operating wavelength ($kd \leq 1$). The effective dielectric permittivity tensor ($\hat{\varepsilon}$) of the structure is determined by combining the Hall permittivity tensor of the semiconductor layer under an external magnetic field (applied along the Y-axis) with the isotropic dielectric constant (ε_d) of the dielectric layer. The alternating semiconductor (d_1) and dielectric (d_2) stacking induces an intrinsic anisotropy along the stratification (Z) direction, resulting in $\varepsilon_{yy} \neq \varepsilon_{zz}$ even in the absence of an external magnetic field. Regarding magneto-optical anisotropy (Hall effect), the application of an external magnetic field H_0 along the Y-axis renders the permittivity tensor of the semiconductor layer non-diagonal and non-symmetric, characteristic of a Hall-type tensor. However, within the effective medium approximation, this Hall tensor effectively reduces to a diagonal but fully biaxially anisotropic tensor for the composite structure ($\varepsilon_{xx} \neq \varepsilon_{yy} \neq \varepsilon_{zz}$) [18]:

$$\begin{pmatrix} \varepsilon_{xx} & 0 & 0 \\ 0 & \varepsilon_{yy} & 0 \\ 0 & 0 & \varepsilon_{zz} \end{pmatrix}, \tag{1}$$

with the components $\varepsilon_{xx}, \varepsilon_{yy}, \varepsilon_{zz}$ equal to [22]:

$$\varepsilon_{xx} = \frac{w^4 a_1 - w^2 a_2 + a_3}{dw^2(w^2 - w_H^2 - w_p^2)}, \quad \varepsilon_{yy} = \frac{w^2(\varepsilon_0 d_1 + \varepsilon_d d_2) - w_p^2 \varepsilon_0}{dw^2}, \quad \varepsilon_{zz} = \frac{\varepsilon_0 \varepsilon_d d(w^4 a_1 - w^2 a_2 + a_3)}{w^4 b_1 - w^2 b_2 + b_3},$$

$$a_1 = d_1 e_0 + d_2 e_d, \quad a_2 = w_H^2 a_1 + w_d^2(d_1 e_0 + a_1), \quad a_3 = d_1 e_0 w_p^4, \quad b_1 = a_1 l_1, \quad l_1 = d_1 e_d + d_2 e_0,$$

$$b_2 = w_H^2 a_1 l_1 + w_p^2 e_0 S, \quad S = (d_2 a_1 + d_1 l_1), \quad b_3 = d_1 d_2 e_0^2 \left(2(w_g^2 + W_p^2) + w_p^4\right).$$

Here e_0 is the lattice dielectric frequency; m_{eff} is the effective mass; $w_H = H_0 e / m_{\text{eff}} c$ is the cyclotron frequency; w_p is the plasma frequency; $w_g = \sqrt{w_H^2 + w_p^2}$ is the hybrid resonance frequency.

Assuming the structure under consideration is non-absorbing ($\vec{J} = 0$, $\rho = 0$), non-magnetic ($\vec{B} = \mu_0 \vec{H}$) and linearly anisotropic ($\vec{D} = \varepsilon_0 \hat{\varepsilon} \vec{E}$. In the frequency domain, Maxwell's equations for harmonic plane waves ($\vec{E}_0 e^{i(\vec{k}\cdot\vec{r} - \omega t)}$) become as follows:

$$\nabla \times \vec{E} = -\frac{\partial \vec{B}}{\partial t} \quad \Rightarrow \quad i\vec{k} \times \vec{E} = i\omega \vec{B} \quad \Rightarrow \quad \vec{k} \times \vec{E} = \omega \vec{B} = \omega \mu_0 \vec{H}, \tag{2}$$

$$\nabla \times \vec{H} = \frac{\partial \vec{D}}{\partial t} \quad \Rightarrow \quad i\vec{k} \times \vec{H} = -i\omega \vec{D} \quad \Rightarrow \quad \vec{k} \times \vec{H} = -\omega \vec{D}. \tag{3}$$

From (2), we have:

$$\vec{H} = \frac{1}{\omega \mu_0} \left(\vec{k} \times \vec{E}\right). \tag{4}$$

Substitute (4) into equation (3), one obtains:

$$\vec{k} \times \left[\frac{1}{\omega\mu_0} \left(\vec{k} \times \vec{E} \right) \right] = -\omega \vec{D}, \tag{5}$$

$$\frac{1}{\omega\mu_0} \left[\vec{k} \times \left(\vec{k} \times \vec{E} \right) - \vec{E}k^2 \right] = -\omega \vec{D}. \tag{6}$$

Multiplying the both sides by $\omega\mu_0$ and setting $k_0^2 = \omega^2\mu_0\varepsilon_0 = \omega^2/c^2$, one comes to the expression:

$$k^2\vec{E} - \vec{k} \times \left(\vec{k} \times \vec{E} \right) = \omega^2\mu_0\vec{D} = \frac{\omega^2}{\varepsilon_0 c^2}\vec{D} = k_0^2\varepsilon_0^{-1}\vec{D}. \tag{7}$$

Due to the relation $\vec{D} = \varepsilon_0\hat{\varepsilon}\vec{E}$, we have:

$$k^2\vec{E} - \vec{k} \times \left(\vec{k} \times \vec{E} \right) = k_0^2\hat{\varepsilon}\vec{E}. \tag{8}$$

Equation (8) in matrix form is as follows:

$$\det \left[\begin{pmatrix} k^2 - k_x^2 & -k_x k_y & -k_x k_z \\ -k_y k_x & k^2 - k_y^2 & -k_y k_z \\ -k_z k_x & -k_z k_y & k^2 - k_z^2 \end{pmatrix} - k_0^2 \begin{pmatrix} \varepsilon_x & 0 & 0 \\ 0 & \varepsilon_y & 0 \\ 0 & 0 & \varepsilon_z \end{pmatrix} \right] = 0. \tag{9}$$

After performing a number of transformations, we obtain a normalized fourth-order equation for k:

$$\frac{k_x^2\varepsilon_x}{k^2 - k_0^2\varepsilon_x} + \frac{k_y^2\varepsilon_y}{k^2 - k_0^2\varepsilon_y} + \frac{k_z^2\varepsilon_z}{k^2 - k_0^2\varepsilon_z} = 0. \tag{10}$$

From Eq. (10), we see that for a given wave propagation direction (with a fixed ratio $k_x : k_y : k_z$), there are always two possible values for the magnitude of the wave vector (k_1 and k_2), corresponding to two orthogonally polarized wave modes in the biaxial medium:

$$k_{1,2}^2 = \frac{-B \pm \sqrt{B^2 - 4AC}}{2A}, \tag{11}$$

with $A = \sum_{i=x,y,z} k_i^2$; $B = k_0^2 \left(\sum_{i \neq j} k_i^2\varepsilon_i\varepsilon_j - k^2 \sum_i \varepsilon_i \right)$; $C = k_0^4\varepsilon_{xx}\varepsilon_{yy}\varepsilon_{zz}$. Here, mode 1 corresponds to the first wave surface, while mode 2 (k_2) corresponds to the second wave surface. The solutions k_1^2 and k_2^2 determine the shapes of the two nested wave surfaces on the iso-frequency surface; both waves exhibit anomalous anisotropic behavior.

3. Dispersion analysis of the n-GaAs/AlGaAs-based biaxial hyperbolic metamaterial

Numerical calculations are performed for the semiconductor–dielectric multilayer structure n-GaAs/AlGaAs: $m_{\text{eff}} = 0.067\, m_0$, $\varepsilon_0 = 12.9$, $\omega_p = 5.3 \times 10^{12}$ rad/s, $\varepsilon_d = 11.8$.

Figure 1 illustrates the frequency dependence of the three components of the effective permittivity (ε_{xx}, ε_{yy}, ε_{zz}). The ε_{yy} component (red dashed line), oriented along the direction of the external magnetic field $\vec{B}$, exhibits the weakest dispersion and remains positive throughout the entire investigated frequency range, indicating that it is only weakly affected by hybrid resonances. In contrast, ε_{xx} (black solid line) and ε_{zz} (blue dotted line) show complex frequency dependences with multiple singularities, providing direct evidence of the BHMM characteristics. The ε_{xx} component exhibits poles where $\varepsilon_{ii} \to \pm\infty$ and zeros where $\varepsilon_{ii} = 0$. For example, ε_{xx} reaches a pole at $\omega \approx 5.6 \times 10^{12}$ s^{-1} (the hybrid resonance frequency) and a zero at $\omega \approx 3.5 \times 10^{12}$ s^{-1} (the effective plasma frequency). The presence of multiple poles and zeros in ε_{xx} arises from the complexity of the analytical expressions and the interlayer coupling, reflecting slow-wave modes characteristic of the layered structure.

The dispersion analysis of biaxial hyperbolic metamaterials (BHMMs) is carried out by means of examining the relationship between the frequency (ω) and the effective permittivity components (ε_{xx}, ε_{yy}, ε_{zz}), identifying the frequency regions where the sign of ε changes, thereby distinguishing between elliptic and hyperbolic dispersion regimes. Fig. 1 shows that ε_{yy} exhibits the weakest dispersion, whereas ε_{xx} and ε_{zz} display pronounced poles and zeros, indicating the strong influence of the hybrid resonance frequency (ω_g) and the plasma frequency (ω_p).

The coexistence of two wave modes (closed and open surfaces) is a characteristic feature of BHMMs. The shape of the iso-frequency surface (IFS) in wave-vector space $\vec{k}$ is classified into two main types according to the sign of the effective permittivity tensor: Type-I hyperbolic dispersion occurs when only one component in the set (ε_{xx}, ε_{yy}, ε_{zz}) is negative, whereas Type-II hyperbolic dispersion arises when two components of the permittivity tensor are negative. From Fig. 1, the structure exhibits Type-I hyperbolic behavior in the frequency range 3.5×10^{12} s^{-1} $< \omega <$ 3.8×10^{12} s^{-1}, with the permittivity components having the sign configuration ($+$, $-$, $+$). The corresponding iso-frequency surface is a double-sheet hyperboloid, compressed in the XZ plane and extended along the Y axis (Fig. 2a). Similarly, in the frequency range 4.9×10^{12} s^{-1} $< \omega < 5.6 \times 10^{12}$ s-1, the structure shows a permittivity sign combination of ($+$, $+$, $-$), where

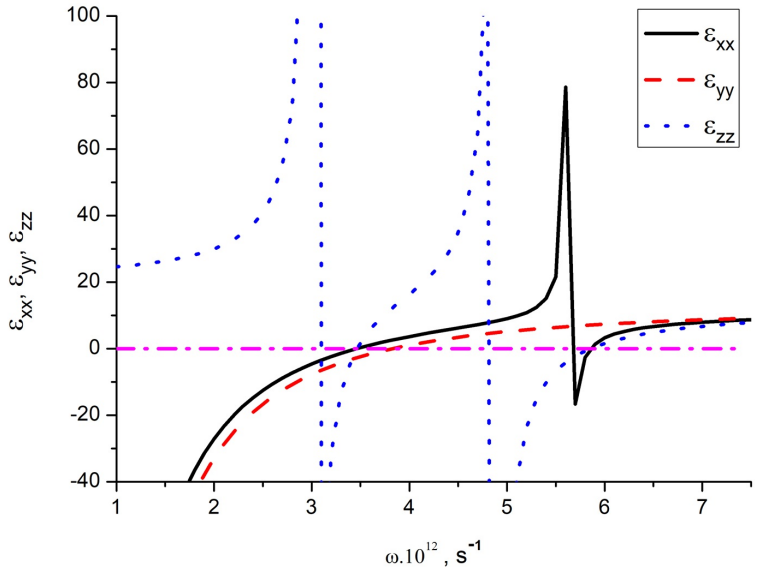

FIG. 1. Spectral dependences of the real parts of effective permittivities ε_{xx}, ε_{yy}, ε_{zz} of metamaterials made of semiconductor–dielectric multilayer structure n-GaAs/AlGaAs with $d_1 = d_2 = 4$ μm.

the iso-frequency surface is strongly compressed in the XY plane and extends infinitely along the Z axis (Fig. 2b). This configuration is highly relevant for hyper-lensing applications and for controlling the photonic density of states (PDOS). The Type-II hyperbolic region (single-sheet hyperboloid) corresponds to $\omega < 3.0 \times 10^{12}$ s^{-1} (Fig. 1). In this range, the permittivity components exhibit the sign configuration $(-, -, +)$, as both ε_{xx} and ε_{yy} take negative values, indicating metallic behavior along the X and Y directions, while retaining dielectric behavior along the Z direction (Fig. 2c). This region allows the propagation of evanescent waves.

The presence of multiple hyperbolic frequency regions indicates that the n-GaAs/AlGaAs BHMM supports multimode operation. The three-dimensional IFS results confirm that, by tuning physical parameters such as the external magnetic field (H_0) and the layer thickness ratio (d_1/d_2), the entire frequency spectrum can be shifted, enabling flexible switching between different BHMM regimes (Type I and Type II). This high degree of tunability is crucial for optimizing the IFS topology, particularly for achieving quasi-flat regions, which are essential for precise beam steering and active THz sensing applications.

The search for near-flat regions on iso-frequency surfaces is a central objective in hyperbolic metamaterial research, as it is directly related to the ability to achieve high-precision control of energy propagation direction, including beam collimation and steering. Based on three-dimensional simulation results obtained from different configurations of ε_{xx}, ε_{yy}, and ε_{zz} (Fig. 3), we analyze the physical conditions leading to the emergence of such near-flat regions. These regions, characterized by vanishing curvature, occur when the IFS is extremely compressed along a confined axis. In the BHMM model, this strong compression arises when the operating frequency ω approaches a pole of the permittivity tensor, causing the magnitude of one permittivity component ε_{ii} to diverge ($\pm\infty$). As shown in Fig. 3b, the $(+, +, -)$ configuration with $\varepsilon = 8.318,\ 4.804,\ -814.889$ provides an optimal condition for achieving near-flatness. Because ε_{zz} attains a very large negative magnitude – several orders of magnitude larger than ε_{xx} and ε_{yy} – this component imposes an extreme compression of the IFS along the Z axis. Under such compression, the two-sheet hyperboloid IFS (Fig. 3b) is flattened into a highly anisotropic structure that lies close to the XY plane. In this strongly confined regime, the dependence of the dispersion relation on k_z becomes negligible, and the IFS asymptotically approaches the form of two parallel planes ($k_z \approx 0$). This pronounced flattening constitutes a clear manifestation of near-flat regions, which are crucial for beam steering applications. For the Type-I hyperboloid opened along the Y direction (Fig. 3a), the $(+, -, +)$ configuration produces a relatively slender geometry with large curvature along the hyperbolic branches, and therefore does not generate sufficiently strong compression to induce surface flattening. In contrast, the single-sheet hyperboloid (Fig. 3c) with the $(-, -, +)$ configuration at frequencies close to the poles of ε_{xx} and ε_{yy} (e.g., $\varepsilon = -147.812, -168.831, 24.659$) develops a bottleneck-like shape, where the hyperbolic branches are strongly stretched and become nearly flat. This near-flatness emerges along the open hyperbolic branches when $|\varepsilon_{xx}|$ and $|\varepsilon_{yy}|$ reach extremely large values ($|\varepsilon_{xx}| \approx 148$, $|\varepsilon_{yy}| \approx 169$). As the IFS undergoes strong stretching, its curvature approaches zero. Fig. 3c clearly illustrates the formation of these tilted planar segments, which are of particular interest for beam steering, since the group velocity vector ($\vec{v}_g$) is always normal to the IFS.

Figure 4 (a and b) illustrate the frequency dependence of ε_{xx} and ε_{yy} for three different values of the applied external magnetic field H_0 (9000 Oe, 7810 Oe, and 3000 Oe). In the considered model, the magnetic field H_0 is applied along the

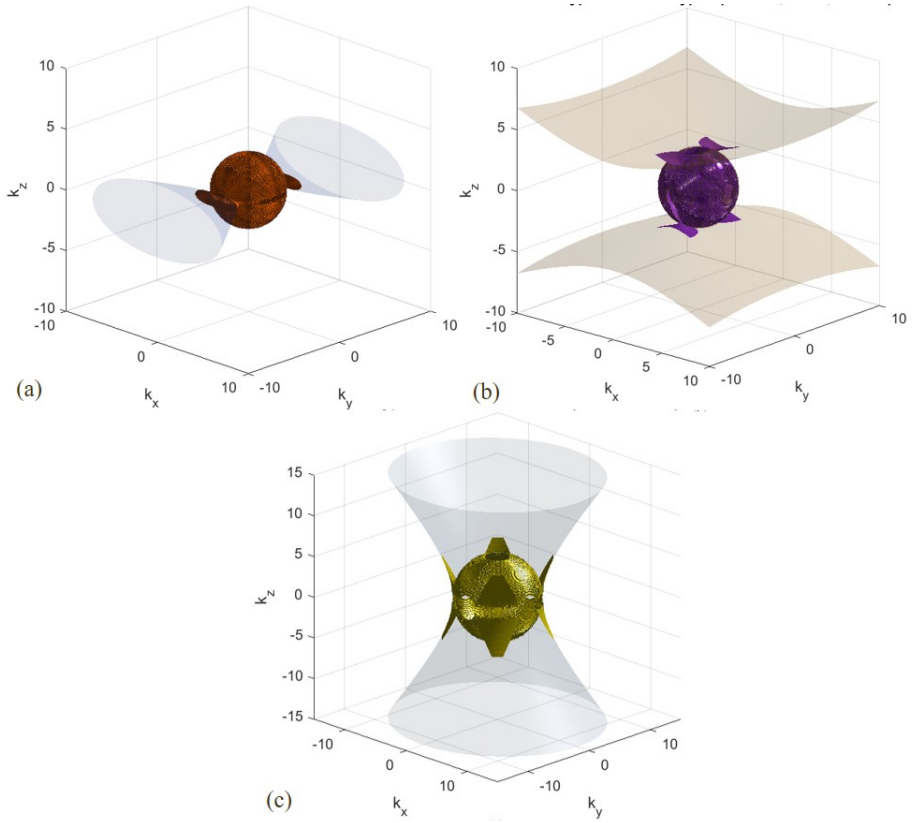

FIG. 2. Iso-frequency surfaces in the wave-vector space for biaxial hyperbolic metamaterials made of semiconductor–dielectric multilayer structure n-GaAs/AlGaAs with $d_1 = d_2 = 4$ μm: a) Biaxial Hyperbolic IFS type I (ε: 1.738; -0.885; 8.928); b) Biaxial Hyperbolic IFS type I (ε: 9.779; 5.384; -39.608); c) Biaxial Hyperbolic IFS dual mode (ε: -42; -50; 27)

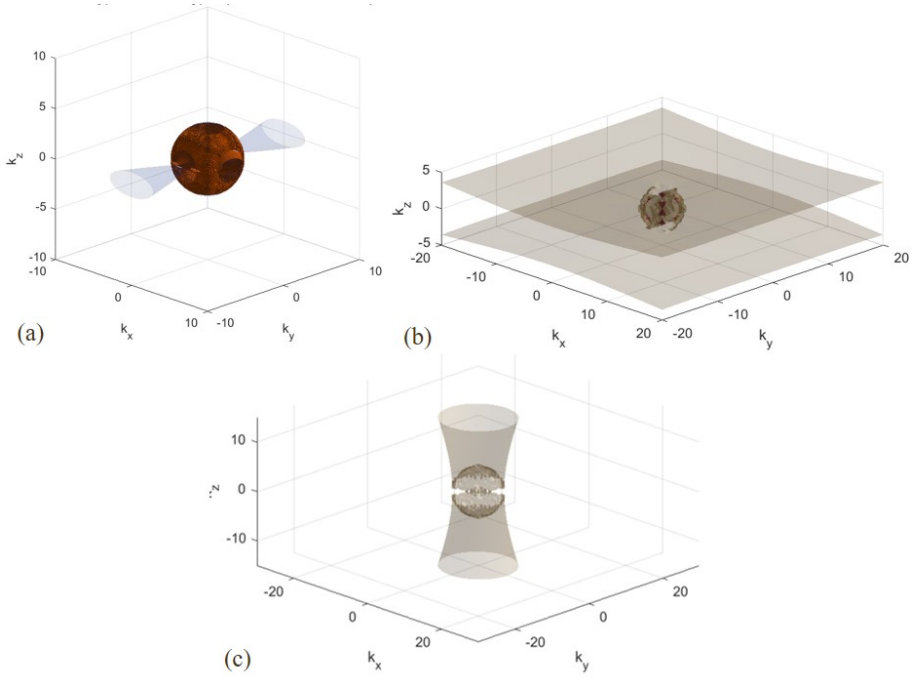

FIG. 3. Iso-frequency surfaces in the wave-vector space for a biaxial hyperbolic metamaterial based on an n-GaAs/AlGaAs multilayer structure ($d_1 = d_2 = 4$ μm), calculated as the operating frequency approaches the zeros – Biaxial Hyperbolic IFS type I (ε: 2.396, -0.197, 11.582) (a) or poles – Biaxial Hyperbolic IFS type I (ε: 8.318, 4.804, -814.889) (b), Biaxial Hyperbolic IFS dual mode (ε: -147.812, -168.831, 24.659) (c) of the effective permittivity tensor components

Y axis. For wave propagation (or electric-field polarization) parallel to the magnetic-field direction, the Hall effect, which is responsible for magnetically induced anisotropy, does not contribute.

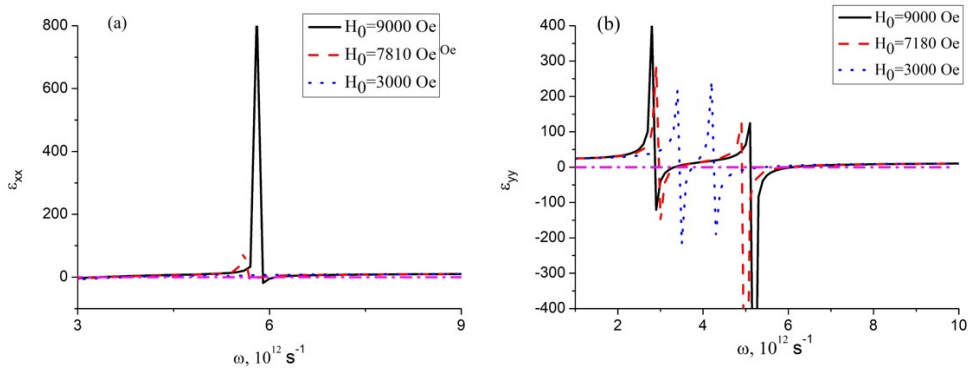

FIG. 4. Spectral dependences of the real parts of effective permittivities ε_{xx} (a), ε_{yy} (b) of metamaterials made of semiconductor–dielectric multilayer structure n-GaAs/AlGaAs ($d_1 = d_2 = 4$ μm) under the influence of an external magnetic field H_0

Nevertheless, both ε_{xx} and ε_{yy} exhibit pronounced shifts in their pole and zero frequencies as H_0 is varied. Specifically, when $H_0 = 9000$ Oe, the pole of ε_{xx} appears at the frequency $\omega = 5.8 \times 10^{12}$ s^{-1}; as H_0 is reduced to 7810 Oe, this pole shifts toward lower frequencies. The magnetic-field dependence of ε_{xx} is more intricate, yet it also displays similar pole–zero shifts, with particularly strong variations occurring around $4.5 - 5.5 \times 10^{12}$ s^{-1}. This behavior can be attributed to the fact that the cyclotron frequency is proportional to H_0. As H_0 decreases, the cyclotron frequency ω_H is reduced, which in turn lowers the hybrid resonance frequency, leading to an overall redshift of the ε_{xx} and ε_{yy} spectra. Consequently, the magnetic-field-induced displacement of the pole and zero frequencies of ε_{xx} and ε_{yy} enable precise control over the positions of the hyperbolic and elliptic dispersion bands. At a fixed operating frequency (e.g., $\omega = 5 \times 10^{12}$ s^{-1}), the material can be switched between elliptic and hyperbolic dispersion regimes simply by tuning H_0.

This switching capability forms the foundation for active sensing devices and modulators. Another important implication is that tuning H_0 enables direct control over the geometric topology of the iso-frequency surfaces. The near-flat regions on the IFS, which are essential for high-precision beam control, emerge when the operating frequency approaches the hybrid resonance frequency ($\varepsilon \to \infty$). By appropriately adjusting H_0, the pole frequency can be shifted to coincide precisely with the desired operating frequency, thereby optimizing the degree of IFS flattening. This tunability allows for the design of BHMM structures capable of efficient energy collimation and directional wave propagation in the THz regime. Similar behavior is also observed when varying the layer thickness ratio from $0.5 \to 2$ (Fig. 5). As the relative thickness of the semiconductor layer increases with respect to the dielectric layer, the average electron concentration within the effective medium is enhanced, leading to a modification of the effective plasma frequency (ω_p^{eff}). The resulting shift in ω_p^{eff} induces a global redshift of the entire dispersion spectrum, further demonstrating the versatility of structural and magnetic-field tuning for controlling BHMM dispersion characteristics.

4. Conclusion

This study confirms the feasibility and advantages of employing n-GaAs/AlGaAs layered structures under an external magnetic field to implement biaxial hyperbolic metamaterials (BHMMs) operating in the THz frequency range. The effective medium approximation (EMA) has been successfully applied, demonstrating that the proposed structure behaves as a BHMM characterized by three distinct effective permittivity components ($\varepsilon_{xx} \neq \varepsilon_{yy} \neq \varepsilon_{zz}$). The analysis reveals that the external magnetic field H_0 serves as a powerful tuning parameter, enabling active switching among different dispersion regimes (elliptic, Type-I hyperbolic, and Type-II hyperbolic) at a fixed operating frequency through controlled shifts of the pole and zero frequencies of ε_{xx} and ε_{yy}. In addition, the layer thickness ratio d_1/d_2 is identified as a key structural design parameter for tailoring the degree of anisotropy and the extreme magnitude of the permittivity components, which ultimately governs the IFS topology. The combined tuning of magnetic and structural parameters demonstrates the ability to generate pronounced near-flat regions on the iso-frequency surfaces, particularly when one permittivity component attains an extremely large magnitude (e.g., $\varepsilon_{zz} = -815$), thereby producing the strong compression required for beam-steering applications. In conclusion, the use of n-GaAs together with its strong magnetically induced tunability establishes this BHMM architecture as a promising platform for next-generation photonic devices, capable of precise manipulation and steering of electromagnetic waves in the THz regime, with significant potential for high-speed communication systems and active sensing applications.

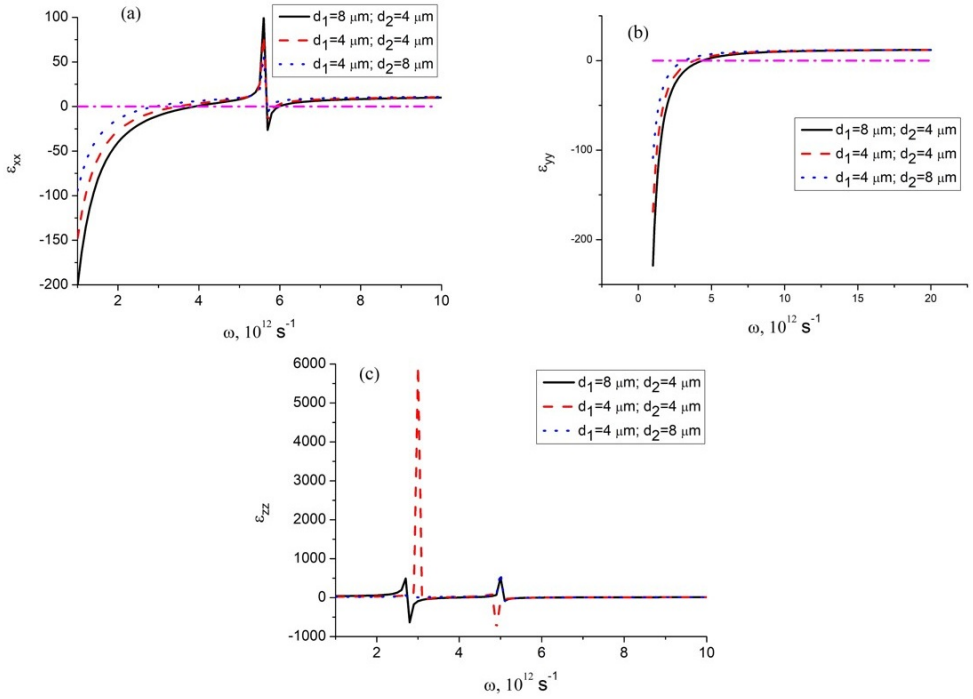

FIG. 5. Spectral dependences of the real parts of effective permittivities ε_{xx} (a), ε_{yy} (b), ε_{zz} (c) under the specified layer thickness ratio (d_1/d_2) of metamaterials made of semiconductor–dielectric multilayer structure n-GaAs/AlGaAs ($d_1 = d_2 = 50$ μm)

References

[1] Veselago V.G. The Electrodynamics of Substances with Simultaneously Negative Values of ε and μ. *Sov. Phys. Uspekhi*, 1968, **10** (4), P. 509–514.
[2] Smith D.R., et al. Metamaterials and Negative Refractive Index. *Science*, 2004, **305** (5685), P. 788–792.
[3] Krushynska A.O., et al. Fundamentals and applications of metamaterials: Breaking the limits. *App. Phys. Lett.*, 2023, **123**, 240401.
[4] Ritchie R.H. Plasma losses by fast electrons in thin films. *Phys. Rev.*, 1957, **106** (5), P. 874–881.
[5] Liu Y., Zhang X. Metamaterials: A new frontier of science and technology. *Chem. Soc. Rev.*, 2011, **40** (5), P. 2494–2507.
[6] Kshetrimayum R.S. A brief intro to metamaterials. *IEEE Potentials*, 2004, **23** (5), P. 44–46.
[7] Yan R., et al. High sensitive plasmonic nanorod hyperbolic metamaterial biosensor. *Photonics Research*, 2022, **10** (1), P. 84–95.
[8] Alù A., Silveirinha M.G., Saladrino A., Engheta N. Epsilon-near zero metamaterials and electromagnetic sources: Tailoring the radiation phase pattern. *Phys. Rev. B*, 2007, **75** (15), 155410.
[9] Chen H.T., et al. Active terahertz metamaterial devices. *Nature*, 2006, **444** (7119), P. 597–600.
[10] Ren Z., et al. Terahertz metamaterials inspired by quantum phenomena. *Research*, 2025, **8** (1), P. 1–28.
[11] Ma Q., Hu H., Huang E., Liu Z. Super-resolution imaging by metamaterial-based compressive spatial-to-spectral transformation. *Nanoscale*, 2017, **9** (46), P. 18268–18274.
[12] Khurgin J.B. Enhanced spontaneous emission inside hyperbolic metamaterials. *Opt. Express*, 2014, **22** (4), P. 4301–4306.
[13] Wang B. X., et al. Review of broadband metamaterial absorbers: From principles, design strategies, and tunable properties to functional applications. *Adv. Func. Mat.*, 2023, **33** (14), 2213818.
[14] Poddubny A., Iorsh I., Belov P., Kivshar Y. Hyperbolic metamaterials. *Nat. Photonics*, 2013, **7**, P. 948–957.
[15] Zheludev N.I., et al. The new phase of light. *Nat. Photonics*, 2020, **14**, P. 337–338.
[16] Chen B., et al. Hyperbolic metasurfaces enable enhancement and regulation of near-field radiative heat transfer. *Int. J. Heat Mass Transf.*, 2025, **169**, 109608.
[17] Chern R.-L, Yu Y.-Z. Chiral surface waves on hyperbolic-gyromagnetic metamaterials. *Opt. Expr.*, 2017, **25** (10), P. 11801–11812.
[18] Bulgakov A.A., Fedorin I. Surface electromagnetic waves in thin-layer biaxial structure in a magnetic field. *J. Electr. Mat.*, 2012, **54**, P. 1566–1574.
[19] Kuznetsov E.V., Merzlikin A.M. Light propagation in a magneto-optical hyperbolic biaxial crystal. *Opt. Comm.*, 2017, **405**, P. 164–170.
[20] Song X., Liu Z., Xiang Y., Aydin K. Biaxial hyperbolic metamaterials using anisotropic few-layer black phosphorus. *Opt. Express*, 2018, **26** (5), P. 5469–5477.
[21] Eylink K. G., et al. Determination of critical parameters for design of semiconductor hyperbolic metamaterials. *Opt. Materials*, 2021, **112**, 110576.
[22] Bulgakov A.A., Fedorin I.V. Electrodynamic properties of a thin-film periodic structure in an external magnetic field. *Opt., Quant. Electr.*, 2011, **56**, P. 510–514.

Submitted 6 January 2026; revised 26 February 2026; accepted 27 February 2026

Information about the authors:

Nguyen Pham Quynh Anh – Faculty of Engineering and Technology, Saigon University, 273 An Duong Vuong Street, Cho Quan Ward, Ho Chi Minh City, Vietnam; ORCID 0009-0009-4001-4873; npqanh@sgu.edu.vn

Conflict of interest: The author declares that he has no potential conflict of interests.